Mechanical properties and damage analyses of fatigue loaded CFRP for tidal turbine applications

Mechanical properties and damage analyses of fatigue loaded CFRP for tidal turbine applications

Parvez Alam, Dimitrios Mamalis, Colin Robert, Austin D. Lafferty, Conchúr Ó Brádaigh
Institute for Materials and Processes, School of Engineering, University of Edinburgh, UK
parvez.alam@ed.ac.uk, d.mamalis@ed.ac.uk, colin.robert@ed.ac.uk, a.lafferty@ed.ac.uk, c.obradaigh@ed.ac.uk

***Abstract*—Tidal turbine blades are routinely subjected to conditions of fatigue loading, which over time results in structural damage that negatively affects blade durability. Structural materials (such as fibre reinforced plastics, FRP) within a tidal turbine blade are therefore of considerable importance, and design parameters for such materials should be reviewed and optimised to decrease fatigue-related losses in strength and stiffness. Carbon fibre reinforced plastics (CFRP) are high strength and stiffness composites that are relatively lightweight compared to other FRP. Here, we characterise the mechanical performance of uni-directional, laminated CFRP using both experimental and computational methods combined. The CFRP are unique as they use powder epoxy rather than standard prepreg or liquid infused. Fatigue damage evolution is detailed using finite element methods. The work provides insights to the engineering design of tidal turbine blades with an aim to improving blade durability.**

Keywords: FRP, Composites, Fatigue, Modelling, Turbines, FEA, Polymer Aging

I. Introduction

The European Commission stipulates three objectives within their climate and energy framework policy, planned for completion by 2030. These include a minimum greenhouse gas reduction of 40%, a minimum share of 27% in renewable energy, and a minimum improvement of 27% in energy efficiency [1]. These objectives can be fulfilled in part, by implementing strategic targets for the design and development of engineered systems to capture and convert naturally available, clean energy resources such as wave, wind and tidal power. The engineering design of efficient wind, tidal and wave energy generating systems is therefore paramount and indeed, vital research is being undertaken to develop e.g. energy storage [2], energy capture [3]–[5], system design [6] and materials [7], [8]. In this paper the focus is on advancing materials technologies for tidal turbine blades.

Engineered materials used in tidal turbine blades are of paramount importance as they influence longevity, durability and blade performance. Factors such as wet corrosion resistance, weight, stiffness and strength all contribute to improved blade performance. At present, glass fibre reinforced plastics (GFRP) are used in bulk to reinforced the spar caps, flanges, outer walls and shear walls of tidal turbine blades. Glass fibres are nevertheless prone to sea water and microbial corrosion [9], [10], which brings into question their suitability for tidal turbine blades. Carbon fibres have contrarily, far superior sea water corrosion resistance [11], [12] as compared to glass fibres and as such there is ongoing work as regards the suitability of replacing GFRP with carbon fibre reinforced plastics (CFRP). Additionally, CFRP is lower weight, higher strength and higher stiffness than GFRP. The primary objection to CFRP use in tidal turbine blades would be in relation to its price. Even an intermediate modulus carbon fibre-epoxy matrix composite is over 3 times more expensive per kg than an E-glass fibre-epoxy composite [13]. As such, the weight saving, mechanical and durability benefits of using CFRP would need to be high to justify the extra cost.

CFRP is often manufactured as carbon fibre prepregs. Thermoset prepregs are typically only partly cured and tend to remain tacky such that storage and handling is not necessarily optimal. In this paper, we consider the use of powder epoxy to fuse carbon fibre tows. Powder epoxy CFRP composites have several potential benefits over prepreg CFRP as they are low cost, have good materials properties, and the manufacturing stages using powder epoxy are reduced. These epoxies melt between 50-100°C, and circumvent chemical curing until a temperature of 150-180°C is reached. As a result, preforming and pre-consolidation is possible at 50-120°C, prior to chemical curing, which is performed separately after the preformed parts are consolidated.

Stress concentrations at composite edges might give rise to premature CFRP fracture. Exposed edges in tidal turbine blades can occur through a combination of cavitation and silt erosion [20]. High tidal-based shear loading encourages local cavitation [21], accelerated water ingress [22] and potential erosion due to silt [23], [24], which weakens the mechanical and fatigue properties of the blade surfaces [26], [27]. This in turn creates surface disparities and micro-cracking. Complex dynamic forces that tidal turbine blades are subjected to are typically high [25] and if edges are exposed, it is possible that composite failure is exacerbated. Seawater ingress in composite materials has been studied extensively. Mechanical property losses due to water diffusion is one of the most critical issues for water immersed composites. Davies et. al. [29] report that there is a significant reduction in strength as a result of water absorption, although moduli and fracture toughness remained unaffected.

This paper is concerned with the mechanical behaviour of powder epoxy based CFRP composites in static tension and in tension-tension fatigue. The objectives are to characterise this mode of failure for powder epoxy unidirectional-CFRP

(UD-CFRP). The intention is to also develop finite element models to simulate the fatigue behaviour of laminated CFRP composites using different fibre orientations. The innovative aspects of this research include (a) failure characterisation of powder epoxy CFRP and (b) the development of a fatigue model to predict failure in CFRP. The importance of this work to tidal turbine blade technology is through ideas towards their design optimisation for an increased service life-span.

II. Materials and methods

A. Manufacture of CFRP coupons

Commercially available continuous tow carbon fibres T700S-24K-F0E (0.7% sizing agent) from TORAYCA (Toray Industries, Inc.), were used as reinforcement material for the composites. A powder epoxy resin (EC-CEP-0016) supplied from EireComposites Teo with a density of 1.22 g/cm^3, was used as the matrix material for the composites. The properties of the carbon fibres are provided in Table I. Unidirectional carbon fibre powder epoxy composites (5-plies) with dimensions of 450 $\times$ 250 $\times$ 1 mm (length $\times$ width $\times$ thickness) were manufactured via a hand lay-up process. The epoxy powder was distributed uniformly on each ply aiming towards a 55:45 (carbon:epoxy) volume ratio. The thermal cycle of all the laminates consisted of a drying stage which is detailed chronologically as follows; isothermal dwell at 50$\pm$ 1 °C for 400 min, B stage; isothermal dwell at 120$\pm$1 °C for 60 min and a curing cycle with a heating rate of 2$\pm$ 0.2 °C/min up to 180$\pm$ 1 °C, holding at this temperature for at least 90 min. At the end of the thermal cycle, the samples were oven cooled to room temperature. The composites were manufactured under vacuum conditions. The specimens were initially placed in a plastic vacuum bag, which was subsequently sealed for isolation from the ambient atmospheric conditions. The samples were compacted by vacuum and a breather cloth was used to remove the air bubbles and volatiles.The fibre volume fractions and void contents of each of the composites (three measurements for each panel) were determined using the acid digestion method (ASTM D3171-2009) [14]. Test coupons were cut and end-tabbed according to BS EN ISO 527-5:2009 [15]. The end tabs were made up of $\pm$45 glass fibre reinforced plastic (GFRP) plates and glued to the CFRP using standard slow setting Araldite adhesive.

TABLE I
PHYSICAL AND MECHANICAL PROPERTIES OF CARBON FIBRES USED TO MANUFACTURE THE COMPOSITES. FROM THE TORAY TECHNICAL DATASHEET CFA-005.

Property	**T700S-F0E-24K Fibre (TORAYCA®)**
Tensile strength (MPa)	4900
Tensile modulus (GPa)	230
Filament diameter (μm)	7
Density (g/cm^3)	1.8
Elongation (%)	2.1

B. Tensile testing and failure analyses

CFRP coupons were subjected to tensile tests using an MTS Criterion Model 45 with a load cell capacity of 333 kN in static mode. Specimens were gripped using 647 hydraulic wedge grips at a pressure of *ca.* 80 bar. Video extensometry (UVX - Imetrum systems) was performed in both axial and transverse loading directions for each test. The camera incorporated into the system is a Manta G-146B/G-146C and is able to video-log at 17.8 frames per second. Testing was conducted at a crosshead rate of 1mm/min and each specimen was loaded to failure. A total of 5 coupons were tested.

C. Fatigue modelling

Fatigue models can be beneficial for developing a design understanding from varied CFRP orientations and layups since tidal turbine blades are routinely subjected to cyclic loads. The fatigue models herein, were developed using Abaqus FEA software (Simulia - Dassault Systemes). The models were constructed as laminated composites using planar shells within a 3-dimensional modelling space. Each laminate was given dimensions of 15 mm by 250 mm. The plies were modelled as orthotropic materials with elastic materials properties provided in Table II. The materials data for the CFRP was obtained from data tables available in the most recent Abaqus tutorial manual.

The moduli were scaled for viscoelasticity in anisotropic materials, and are implemented for elements that behave as linear elastic materials i.e. they have not reached or exceeded a defined failure stress (refer to Table II). Anisotropic viscoelastic scaling, expressed as relaxation coefficients, can be somewhat simplified via Equations 1 and 2. Here $\bar{D}$ is the elasticity tensor and K is a bulk modulus parameter derived from the elastic moduli and Poisson's ratio, ν. Using a single-dimensional case for the sake of simplicity, $K = E/3(1-2\nu)$. $\bar{g}_k^P$ and $\bar{k}_k^P$ are normalised shear and bulk compliances, expressed as a function of time. Loading is sinusoidal and as such the fatigue properties reflect the oscillatory material responses.

$$\bar{D}_\infty = \bar{D}_0(1 - \sum_{k=1}^{n} \bar{g}_k^P) \tag{1}$$

$$K_\infty = K_0(1 - \sum_{k=1}^{n} \bar{k}_k^P) \tag{2}$$

The elasticity matrix, scaled for viscoelasticity is then updated to include an Azzi-Hill-Tsai damage model, Equation 3, where σ_{11} is the tensile/compressive stress in the fibre axis, σ_{22} is the tensile/compressive stress in the transverse to fibre axis, τ_{12} is the shear stress, S_{Lt} is the tensile strength in the fibre axis, S_{Tt} is the transverse to fibre axis tensile strength and S_{LTs} is the in plane shear strength. As long as this criterion holds a value below unity, the composite properties only change as a function of viscoelastic scaling. Once any area (e.g. within an element) of the composite reaches unity, that area incurs damage while the rest of

the model remains viscoelastic. The material responses are calculated via Equation 4, which includes an updated elasticity matrix for damage, D_u, and retains the real-time vectors for stress and strain, σ and ϵ, respectively.

$$\frac{\sigma_{11}^2}{S_{Lt}^2} + \frac{\sigma_{22}^2}{S_{Tt}^2} + \frac{\sigma_{11}\sigma_{22}}{S_{Lt}^2} + \frac{\tau_{12}^2}{S_{LTs}^2} = 1 \tag{3}$$

$$\sigma = D_u \epsilon \tag{4}$$

Further to these parameters, fatigue failure stresses and strains are given growth rates of 1 MPa/0.01 strain (initial) and 2 MPa/0.05 strain (thereafter) resulting in plastic strains that develop in the material after a stress value corresponding to the maximum tensile stress has been reached. Layups of 0°/45°/90°/-45° and 0°/0°/0°/0° were simulated and compared using 1.5 mm thick plies. Failure strengths were incorporated into the models and were dependent upon the magnitudes of local straining within the composite. An initial stress of 2 GPa was applied to one end of the laminated system, and the opposite end was assigned a Dirichlet (fixed) boundary. A modified Newton method coupled to a Fourier series representation was used to define cyclic responses at 5 Hz, which is the standard frequency advised in experimental fatigue as it does not result in heat induced changes to the polymer [8]. Here we use a displacement function u to define the response of the CFRP laminate over times t within a load cycle period T such that $u(t)$ is equal to $u(t+T)$, favouring thus, the truncated Fourier series in Equation 5; where n is the number of Fourier series terms, ω is the angular frequency and is equal to $2\pi/T$, and u_0, u_k^s, u_k^c are displacement coefficients. The fundamental form by which means Newtons methods are used to solve nonlinear equilibrium equations can be represented by Equation 6. Here, $F(t)$ represents a discretised cyclic load such that $F(t) = F(t+T)$ over all times, t through a load cycle period, T. The internal force vector is represented by $I(t)$ and $R(t)$ is the residual vector. The residual vector can be expanded within a modified Newton method ($\bar{R}$) using a Fourier series of the same form as the displacement solution, Equation 7. Here, R_0, R_k^s, R_k^c in the Fourier series are residual vector coefficients that correspond to the displacement coefficients u_0, u_k^s, u_k^c in Equation 5. The residual vector is then obtained via discretised (elemental) calculations via the Fourier coefficients (Equations 8-10), which are integrated over each cycle.

$$u(t) = u_0 + \sum_{k=1}^{n} [u_k^s \sin k\omega t + u_k^c \cos k\omega t] \tag{5}$$

$$R(t) = F(t) - I(t) = 0 \tag{6}$$

$$\bar{R}(t) = R_0 + \sum_{k=1}^{n} [R_k^s \sin k\omega t + R_k^c \cos k\omega t] \tag{7}$$

$$R_0 = \frac{2}{T} \int_0^T R(t) dt \tag{8}$$

$$R_k^s = \frac{2}{T} \int_0^T \sin k\omega t dt \tag{9}$$

$$R_k^c = \frac{2}{T} \int_0^T \cos k\omega t dt \tag{10}$$

TABLE II
CFRP MECHANICAL PROPERTIES USED AS FATIGUE MODEL INPUT PARAMETERS.

Material Property	Value
Elastic modulus (axial, 1) [GPa]	155
Elastic modulus (transverse, 2) [GPa]	12
Poisson's ratio	0.25
Shear Modulus (12) [GPa]	4.4
Shear Modulus (13) [GPa]	4.4
Shear Modulus (23) [GPa]	3.2
Tensile strength (axial, 1) [GPa]	2.3
Compressive strength (axial, 1) [GPa]	1.2
Tensile strength (transverse, 2) [GPa]	0.051
Compressive strength (transverse, 2) [GPa]	0.021
Shear strength [GPa]	0.099

III. RESULTS

The fibre volume fraction in the centre of each panel was on average 54%. Higher fractions were apparent at the edges of each panel and only central regions of each panel were used for tensile testing. The tensile properties of coupons are provided in Table III and individual stress-strain curves for this series are provided in Figure 1.

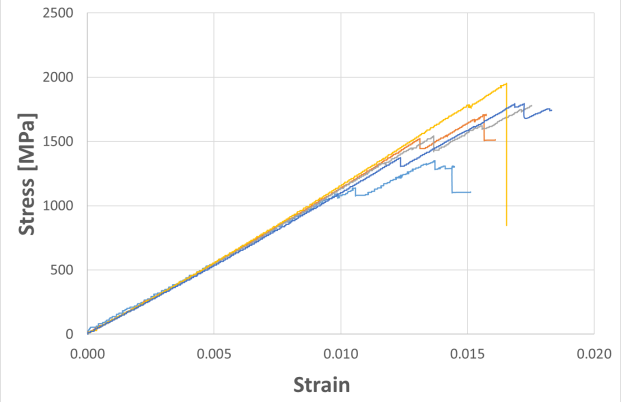

Fig. 1. Tensile stress-strain curves for each coupon.

The moduli and strength values of the CFRP coupons tested herein are within the upper 30th percentile for CFRP composites [16]. Moreover, on observation of the stress-strain curvatures in Figure 1, signs of early failure are evident in some of the curves as there are reductions in stress prior to final fracture. It is likely that any damage that might arise at the edges from cutting will detrimentally affect mechanical performance. Using both transverse and axial strain readings

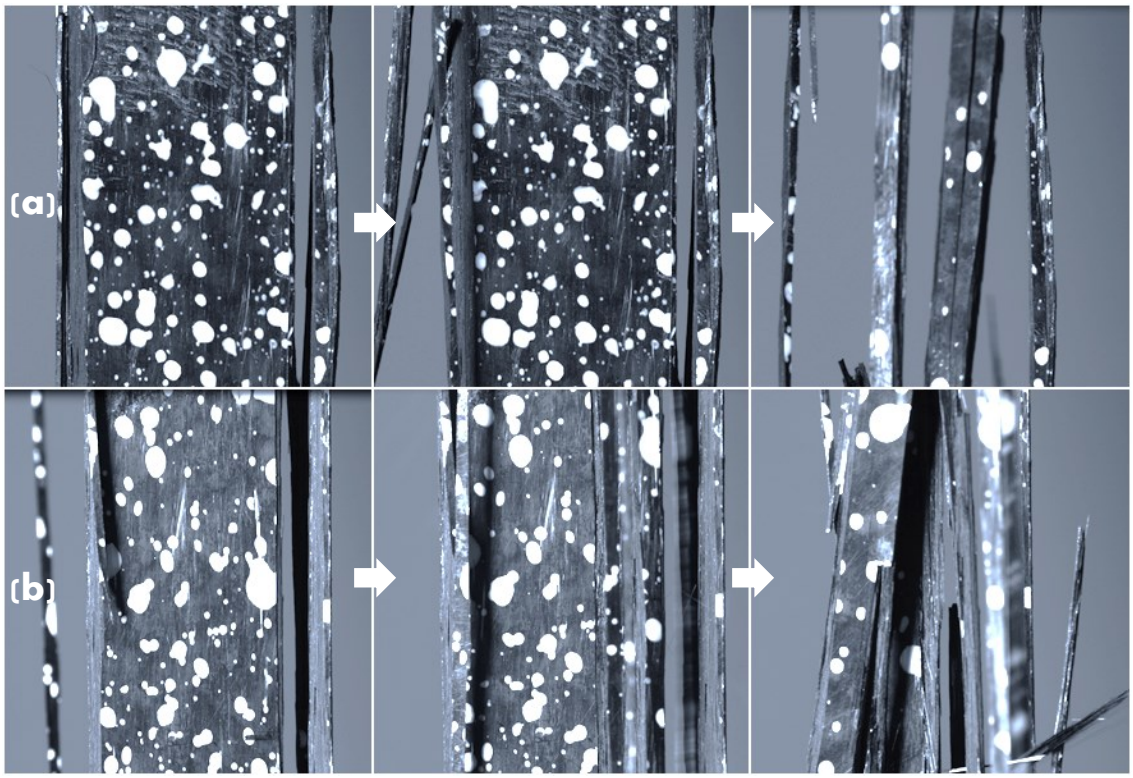

Fig. 2. Video extensometer frame captures showing representative examples of axial fractures in (a) coupon 1 and (b) coupon 4. The increase in axial fracture in these coupons is a function of load and the tendency in these samples is for fracture to begin at the edges and continue towards the centre. The figure shows just the front face of each sample and the progression of fracture over time (from left to right for each of (a) and (b)).

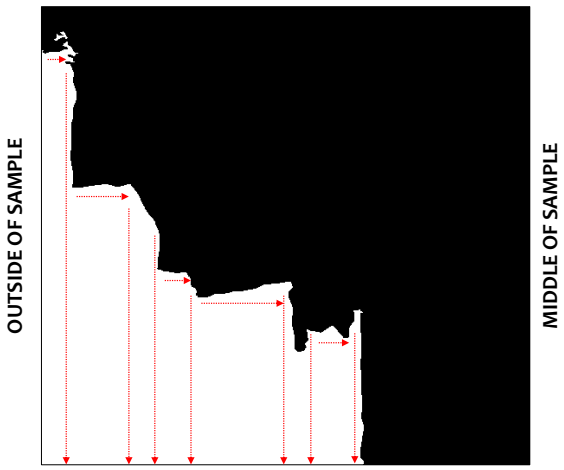

Fig. 3. Binary image of half the width of a coupon showing an edge to centre fracture path. The dotted arrows indicate primary directions of transverse crack propagation leading to the axial fractures seen in Figure 2.

from the video extensometer, we find that the Poisson's ratio for each composite tested was *circa* 0.4.

TABLE III
TENSILE PROPERTIES OF MANUFACTURED UD-CFRP.

	Tensile Modulus [GPa]	**Tensile Strength [MPa]**
Median	112	1777
Mean	109.6	1712
Standard deviation	10.3	224
Coefficient of variation	0.1	0.1

Each tensile coupon failed in an explosive manner with fracture lines running predominantly along the fibre axis. These fracture lines presumably initiate from partial transverse fractures and we suggest that the axial fractures are a function of diverted fracture energies along fibre-matrix interfaces, where fracture energies may more easily dissipate. Figure 2, taken from the extensometer video footage, provides a close-up view of cumulative axial fractures from the early to the latter stages of testing for two of the five coupons tested. In this figure, we note that axial fractures begin on the outermost edges of the CFRP coupons and work their way inwards, indicating that transverse fracture starts from the edges after which fracture energy is redirected along the fibre axis, after

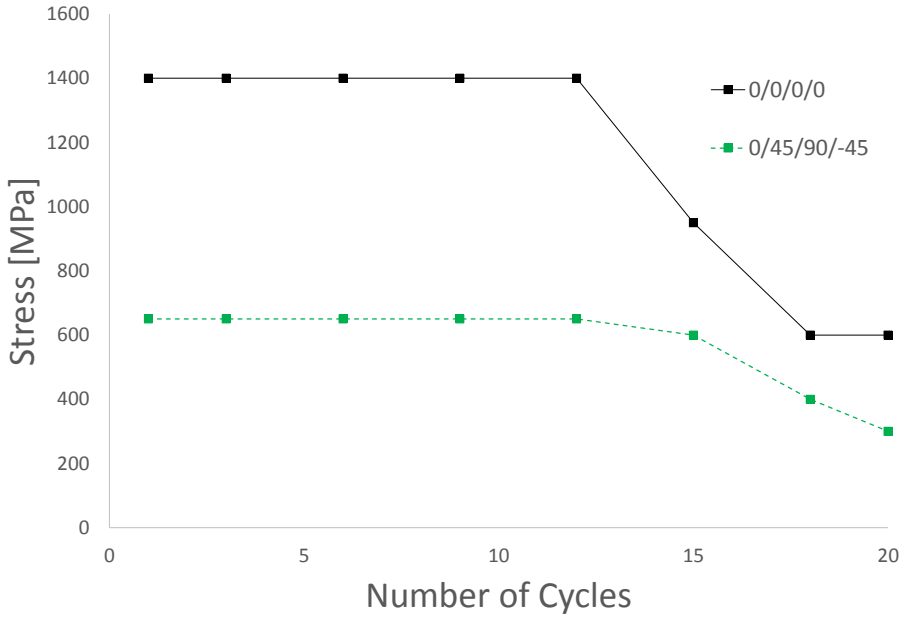

Fig. 4. Fatigue modulus reduction against the number of loading cycles as predicted by our FE model. The simulations are high stress (low cycle) fatigue.

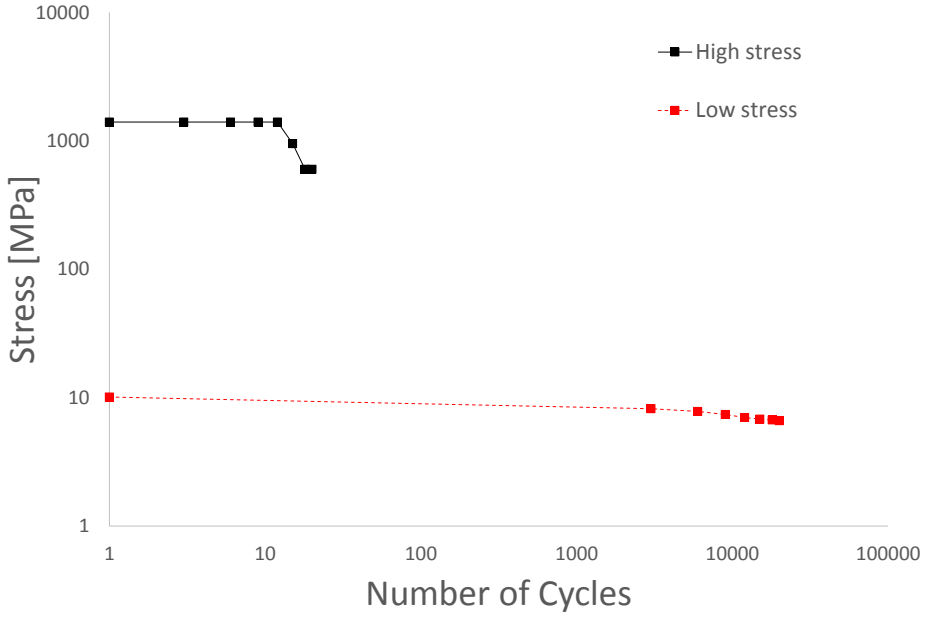

Fig. 5. Fatigue modulus reduction against the number of loading cycles as predicted by our FE model. The simulations include both high stress (low cycle) and low stress (high cycle) fatigue.

which the transverse fracture to axial fracture cycle repeats. The result is a step-wise cross-fracture profile, an example of which is shown as a binary image of a fracture line across the width of a coupon, Figure 3. Individual fractures occur

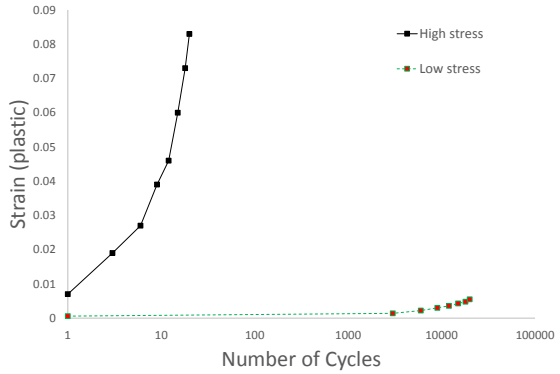

Fig. 6. Plastic strains against the number of loading cycles as predicted by our FE model. The simulations include both high stress (low cycle) and low stress (high cycle) fatigue.

as a function of loading and thus time, and are the cause of the reductions in load carrying capacity observed in Figure 1 to occur part-way through the tensile tests. High strain energies typically arise at coupon edges and are a function of transverse straining. If the strain energy exceeds a critical value for fibre fracture, then fibres will break, releasing fracture energy to neighbouring fibres and allowing a transverse crack to propagate. Rosen [17] and Zweben [18] attribute transverse fractures to flaws in the fibre lengths, and to ineffective fibre lengths (i.e. fibres that are not as long as the entire coupon, or gaps between fibres within the length of a coupon). In their reports nevertheless, they evidenced the build up of axial fractures *prior* to complete UD composite failure. This is a characteristic that was not visually evident from our UD coupons and for that reason, alongside the evident movement of axial fractures from edge to centre (refer to Figures 2 and 3), we suggest strain energy build up at the edges as being causative to coupon failure. Purslow [19] identifies a very large range of possible failure mechanisms in UD-CFRP composites. Based on Purslow's observations, it would seem that transverse fibre failures can be attributed fibre nearness, such that radiating fracture energies from one fibre actually are able to reach neighbouring fibres with sufficient intensity to cause the neighbouring fibres to fracture in a similar fashion to the original (neighbour) fibre fracture. This mechanism of fibre-to-fibre fracture is possible if fibres are close, and are brittle. If the distance between fibres exceeds a critical distance, fracture energies passes through the ductile/amorphous matrix matter, and fracture energies become dispersed (and the primary force scalars may change direction). If nevertheless, fracture energies are sufficiently high to cause debonding of the fibre as they change direction, then fracture can proceed along the fibre axis as opposed to transversely across the fibres. Besides large distances between fibres (essentially, irregularities in fibre distribution), other potential reasons for why fracture energies may change direction can include; fibre flaws, fibre misalignment, small or large voids/inclusions, and non-wetted fibre surfaces.

Figure 4 shows how the peak tension-tension fatigue stress decreases as a function of the number of cycles in both 0°/0°/0°/0° and 0°/45°/90°/-45° CFRP composites, as predicted by our FE models. The stress levels for 0°/0°/0°/0° CFRP are considerably higher than for the 0°/45°/90°/-45° composites and this is expected since the level of load resistance in UD-CFRP is more effective than in fibre composites where the fibres are not aligned with the loading axis. As fibres become more misaligned with the loading axis, there is a progressively greater contribution to loading resistance from the polymeric matrix component of the composite. Figure 5 shows how the peak tension-tension fatigue stress varies in 0°/0°/0°/0° composites when subjected to both high stress (low cycle) and low stress (high cycle) cyclic loading. The predictions are logical in that under high stress (low cycle) fatigue, stress (and thus the load carrying capacity of the composite) is reduced at a more rapid rate as a function of cycling. Further, under low stress (high cycle) fatigue, there is very little variation in the fatigue stress, though there is a noticeably small reduction in stress between 9000 and 20,000 cycles. The fatigue responses in Figures 4 and 5 invariably relate to the extent of irrecoverable composite damage. A correlation between composite damage (plastic straining) and stress reduction as a function of cycling is made evident from Figure 6. In this figure, the plastic straining within the 0°/0°/0°/0° composite is plotted against the number of cycles of load for both high stress and low stress fatigue cases. It is obvious from this figure that considerably more irrecoverable damage (plastic straining) occurs under the duress of high stress fatigue than under low stress fatigue. This said, at present his model has not been validated against experimental data and as such should be considered prototypical at present.

IV. Discussion and Context

This work comprises a preliminary investigation into the effects of fatigue loading on CFRP for tidal turbine applications. Fatigue models have been developed for the purpose of predicting the effects of typical composite lay-ups and their role in the fatigue behaviour of laminated CFRP. In this case 0°/0°/0°/0° and 0°/45°/90°/-45° lay-ups were deemed representative of typical composite ply orientations found in engineered structures, and can be considered small unit-cells by which means larger scale components can be manufactured. As such, the models are currently only prototypical in nature, and example material properties available within the simulation software have been used. A fundamental-level of verification of the model has been possible and we note that the model converges without any numerical problems. Nevertheless, representative empirical input data that corresponds to the fatigue stress-strain behaviour of powder epoxy CFRP must be obtained in order to (a) generate simulation data that is more realistically tuned to the properties of the CFRP we are testing, and (b) verify the veracity of the model predictions and hence modelling approach, against experimental values.

The initial experimental work in this paper focused on the static tensile response of uni-directional CFRP coupons (0°/0°/0°/0°). The results suggest that material failure occurs via an edge to centre transverse fracture mechanism, rather than via axial fractures, which we had expected from a uni-directional CFRP coupon test. As suggested by these results, this is possibly due to flaws in cut edges potentially including; discontinuities in the composite edges (acting as crack initiation sites) and fibre misalignment from the sample preparation process leading to discontinuous fibres at the coupon edges. In an axial static test, discontinuous fibres at the sample edges will reduce the effective cross-sectional area of the sample being tested. These edge effects combined with possible fibre misalignments yield results that have a higher level of statistical scatter than expected.

Our initial observations have laid the groundwork for a continuation study of the environmental effects of aging on the properties of novel powder epoxy CFRP composites with respect to edge defects.

V. Future Work

Our continuation plans for research are to understand the failure mechanisms of materials with respect to environmental conditions, and to generate comprehensive experimental properties results with that will be used to validate and refine the prototypical fatigue models described herein.

VI. Conclusions

Hand laid powder epoxy UD-CFRP were found to have tensile strength and modulus values of *ca.* 1700 MPa and 110 GPa, respectively. An analysis of the fracture profiles of the individual coupons has led us to postulate that transverse (cross-fibre) fractures initiate at the edges and work their way inwards. Transverse cracking subsequently leads to axial fracture, and these axial fractures are used as evidence to edge-to-centre fracture mechanisms. These findings are important in the design of tidal turbine blades as edges may be initiation points for fracture and as such, designers should re-consider methods of blade manufacture in order to minimise cut edges, especially in areas of high stress. Blade design should also consider methods by which damage to blade surfaces can be reduced. Fatigue models were developed with the aim to compare and contrast the stress-cycle behaviour of UC-CFRP given variable lay-ups and different load-amplitudes. The models yield logical results, and their comparison against experimental test results is planned as further research.

Acknowledgments

The authors would like to acknowledge the European Union for funding this research through the following projects: MARINCOMP, Novel Composite Materials and Processes for Marine Renewable Energy, Funded under: FP7-People, Industry Academia Partnerships and Pathways (IAPP), Project reference: 612531. POWDERBLADE, Commercialisation of Advanced Composite Material Technology: Carbon-Glass Hybrid in Powder Epoxy for Large Wind Turbine Blades, Funded under: Horizon 2020, Fast Tract to Innovation Pilot, Project reference: 730747.

References

[1] "2030 Climate and Energy Framework". *European Commission*: https://ec.europa.eu/clima/policies/strategies/2030en (seen 12.04.2017)

[2] R.M. Dell and D.A.J. Rand. "Energy storage a key technology for global energy sustainability." *Journal of Power Sources*, vol. 100 pp. 217, 2001

[3] A. Kusiak and Z. Song. "Design of wind farm layout for maximum wind energy capture." *Renewable Energy*, vol. 35 pp. 685-694, 2010

[4] K.E. Johnson, L.Y. Pao, M.J. Balas and L.J.Fingersch. "Control of variable-speed wind turbines: standard and adaptive techniques for maximizing energy capture." *IEEE Control Systems*, vol. 26 pp. 70-81, 2006

[5] J.A.M. Cretel, G. Lightbody, G.P. Thomas and A.W. Lewis "Maximisation of energy capture by a wave-energy point absorber using model predictive control." *IFAC Proceedings Volumes*, vol. 44 pp. 3714-3721, 2001

[6] Z. Salameh. "Renewable Energy Systems Design." Elsevier Inc. 2014

[7] P. Davies. "Environmental degradation of composites for marine structures: new materials and new applications." *Philosophical Transactions of the Royal Society A*, vol. 374 pp. 20150272, 2016

[8] C.R. Kennedy and C. Ó Brádaigh. "Immersed fatigue performance of glass fibre-reinforced composites for tidal turbine blade applications." *Journal of Bio- and Tribo-Corrosion*, vol. 2 pp. 11-12, 2016

[9] H. Gu. "Tensile behaviours of quartz, aramid and glass filaments after NaCl treatment." *Materials and Design*, vol. 30 pp. 867-870, 2009

[10] H. Staudigel, R.A. Chastain, A. Yayanos and W. Bourcier. "Biologically mediated dissolution of glass." *Chemical Geology*, vol. 126 pp. 147-154, 1995

[11] N. Zhuang, Y. Zhou, Y. Ma, Y. Liao and D. Chen. "Corrosion activity on CFRP-strengthened RC piles of high-pile wharf in a simulated marine environment." *Advances in Materials Science and Engineering*, vol. 2047 pp. 7185452, 2017

[12] Y. Nakai and C. Hiwa. "Effects of loading frequency and environment on delamination fatigue growth of CFRP." *International Journal of Fatigue*, vol. 28 pp. 155-159, 2002

[13] M.G. Bader "Selection of composite materials and manufacturing routes for cost-effective performance." *Composites: Part A*, vol. 33 pp. 913-934, 2002

[14] ASTM D3171-09, "Standard Test Methods for Constituent Content of Composite Materials", *ASTM International*, West Conshohocken, PA, 2009

[15] BS EN ISO 527-5 "Plastics - Determination of tensile properties Part 5: Test conditions for unidirectional fibre-reinforced plastic composites." *European Committee for Standardisation*, 2009

[16] V. Narula, V. Jain, M.F. Khan and S. Bahuguna. "Review on mechanical properties of carbon epoxy in context of best material selection." *The Engineering Journal of Application and Scopes*, vol. 2 pp. 14-19, 2017

[17] B.W. Rosen. "Tensile failure of fibrous composites." *AIAA Journal*, vol. 2 pp. 1985-1991, 1964

[18] C. Zweben. "Tensile failure of fibre composites." *AIAA Journal*, vol. 6 pp. 2325-2331, 1968

[19] D. Purslow. "Fractogrpahic analyses of failures in CFRP." *AGARD Conference Proceedings No. 355, Characterisation, Analysis and Significance of Defects in Composite Materials*, 56th Meeting of the Structures and Materials Panel in London, UK 12-14 April 1983.

[20] P.P. Gohil and R.P. Saini. "Coalesced effect of cavitation and silt erosion in hydro turbines - a review." *Renewable and Sustainable Energy Reviews*, vol. 33 pp. 280-289, 2014

[21] R.F. Nicholls-Lee, S.R. Turnock and S.W. Boyd. "Simulation based optimisation of marine current turbine blades." In: *7th International Conference on Computer and IT Applications in the Maritime Industries (COMPIT'08)*, Liege, Belgium pp. 314-28, 21-23 Apr 2008

[22] A.A. Fahmy and J.C. Hurt. "Stress dependence of water diffusion in epoxy resin." *Polymer Composites*, vol. 1 pp. 7780, 1980

[23] Y. Fouad, M. El-Meniawi and A. Afifi. "Erosion behaviour of epoxy based unidirectional (GFRP) composite materials." *Alexandria Engineering Journal*, vol. 50 pp. 2934, 2011

[24] K. Tsuda, M. Kubouchi, T. Sakai, A.H. Saputra and N. Mitomo. "General method for predicting the sand erosion rate of GFRP." *Wear*, vol. 260 pp. 10451052, 2006

[25] B. Gaurier, P. Davies, A. Deuff and G. Germain. “Flume tank characterization of marine current turbine blade behaviour under current and wave loading.” *Renewable Energy*, vol. 59 pp. 1-12, 2013

[26] D.M. Grogan, S.B. Leen, C.R. Kennedy and C. O Bradaigh. “Design of composite tidal turbine blades.” *Renewable Energy*, vol. 57 pp. 151-162, 2013

[27] H.I. Gonabadi, N. Moharrami, A. Oila and S.J. Bull. “Wet flexural fatigue behaviour of tidal turbine blade composite materials.” In: *11th European Wave and Tidal Energy Conference, Nantes, France*, 2015

[28] W. Shi, M. Atlar, R. Rosli, B. Aktas and R. Norman. “Cavitation observations and noise measurements of horizontal axis tidal turbines with biomimetic blade leading-edge designs.” *Ocean Engineering* , vol. 121 pp. 143155, 2016

[29] N. Tual, P. Carrere, P. Davies, T. Bonnemains and E. Lolive. “Characterization of sea water ageing effects on mechanical properties of carbon/epoxy composites for tidal turbine blades.” *Composites Part A: Applied Science and Manufacturing*, vol. 78 pp. 380389, 2015